

PHASE-SENSITIVE LBIC ANALYSIS

Th. Pernau, P. Fath
 Universitaet Konstanz, Fachbereich Physik, Fach X916, D-78457 Konstanz, Germany
 Tel.: +49-7531-88-3644, Fax: +49-7531-88-3895

ABSTRACT: We investigated the phase shift in light beam induced current (LBIC) maps of silicon solar cells. The phase shift introduced by the solar cell depends on carrier lifetime, carrier diffusion velocity, time delay in both instrument and sample and the impedances incorporated in the solar cell itself. At a reference frequency of 1 kHz, the phase shift introduced by carrier lifetime and diffusion dynamics is around 1°, the solar cell's internal capacitors and resistors introduce a phase shift of up to 70°. Significant structure in phase maps is only visible in the long wavelength range (833 nm, 910 nm and 980 nm).

Keywords: LBIC – 1, Spectral response – 2, Lifetime – 3

1. INTRODUCTION

The light beam induced current (LBIC) technique is a spatially resolving characterisation method for any photosensitive device. The sample, i.e. a solar cell, is illuminated by a small light spot and the generated photocurrent or photovoltage is measured. By moving either the light spot or the sample, it is possible to record a topography. If the signal is detected by lock-in amplifiers, it is also worth looking at the phase shift introduced by the experiment. Inspired by the theory of modulated free carrier absorption (MFCA) [1], we focused on the conditions given by a solar cell.

2 THE LBIC SETUP

In our LBIC setup, the sample is illuminated by four amplitude-modulated diode lasers with wavelengths of 635 nm, 835 nm, 910 nm and 980 nm coupled into one optical fibre. The amplitude modulation of the lasers at different frequencies enables easy separation of the solar cell's response as well as reflection signal $R(\lambda)$ captured by the reflection measurement cells. $I_{sc}(\lambda)$ is measured using a current-to-voltage converter whereas for photovoltage measurements, the sample is directly connected to the voltage input of the lock-in amplifiers. The dual-phase lock-in amplifiers not only give signal magnitude readout, they also provide information about signal time shift, which is expressed in terms of a phase shift ϕ .

More details of our experimental setup can be found in [2], further LBIC systems are described in [3, 4, 5, 6, 7, 8, 9].

3 DETECTION OF PHASE SHIFT

3.1 Signal processing with the lock-in amplifier

The lock-in amplifier is a phase and frequency sensitive AC signal analyser which enables individual signal extraction out of a sum of AC signals, even if large DC offsets or noise are present.

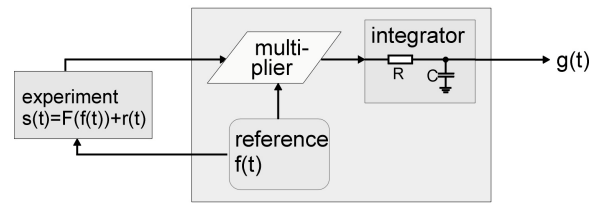


Fig. 1: Schematic of a basic lock in unit, known as one-phase lock-in amplifier. The signal $s(t)$ is multiplied with the reference $f(t)$ and integrated over a time span T_c , which is called the time constant of the lock-in amplifier.

The lock-in amplifier commonly has a built-in reference oscillator, which is generating the reference

$$(1) \quad f(t) = \sin(\omega_{ref}t) + C$$

C is an arbitrary offset. The experiment is fed with the reference as input parameter. The reaction is a function of the reference plus noise ($r(t)$):

$$(2) \quad s(t) = F(f(t)) + r(t)$$

For further analysis, we have to look at the Taylor series of $F(f(t))$:

$$(3) \quad F(f(t)) = F(C) + \sin(\omega_{ref}t) \cdot F^{(1)}(C) + \frac{1}{2!} (\sin(\omega_{ref}t))^2 \cdot F^{(2)}(C) + \dots$$

Where $F^{(i)}$ means $\frac{\partial^i F(f)}{\partial f^i}$

If the response of the experiment is linear, i.e. $F(x) = B \cdot x$, then (3) reduces to:

$$(4) \quad F(f(t)) = B \cdot C + B \cdot \sin(\omega_{ref}t + \phi)$$

Note that ϕ is a phase shift between the signal component and the reference, caused by the experiment, cabling etc.

The multiplication followed by an integration in the lock-in amplifier corresponds to a correlation function:

$$(5) \quad g(t_0) = \frac{1}{T_c} \int_{t_0}^{t_0+T_c} f(t) \cdot s(t) dt$$

where t_0 is the time when the readout is taken. The integral may be split into three parts:

$$(6) \quad g(t_0) = CB \frac{1}{T_c} \underbrace{\int_{t_0}^{t_0+T_c} \sin(\omega_{ref} t) dt}_0 + \frac{1}{T_c} \underbrace{\int_{t_0}^{t_0+T_c} r(t) \cdot \sin(\omega_{ref} t) dt}_0 + \frac{B}{T_c} \int_{t_0}^{t_0+T_c} \sin(\omega_{ref} t) \cdot \sin(\omega_{ref} t + \varphi) dt$$

The first term which contains the offset is cancelled out if or if T_c is large enough, as the sine term is a symmetrical signal. The second term in (6) belongs to the random noise and is cancelled out under the same conditions as the first term, as the random noise times a symmetrical signal is also symmetrical. The last term of (6) is the interesting signal and computes to:

$$(7) \quad \frac{1}{2} B \cos \varphi$$

3.2 The two-phase lock-in amplifier

The basic lock-in's readout (7) depends on the phase shift φ , which may change. To overcome this problem, most lock-in amplifiers use two basic lock-in units driven by one reference, see Fig. 2.

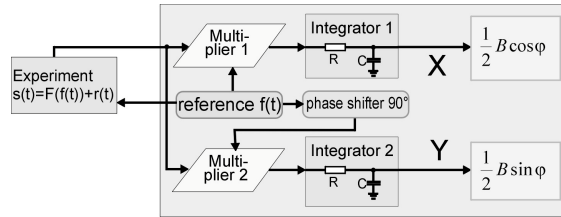


Fig. 2 : The two-phase lock-in amplifier consists of two lock-in units driven by the same reference, but with a phase shift of 90° in the second channel. The vector outputs X and Y are used to separate magnitude and phase, see text.

The vector outputs X and Y of the two-phase lock-in amplifier contain the real and imaginary part of the experiment's response. The magnitude (R) and phase (φ) readout of the two-phase lock-in amplifier is then:

$$(8) \quad R = \sqrt{x^2 + y^2} \quad \text{and} \quad \varphi = \arctan\left(\frac{y}{x}\right)$$

4 INFLUENCE OF SOLAR CELL PARAMETERS ON PHASE SHIFT

4.1 Bulk lifetime / diffusion length

Consider a solar cell submitted to monochromatic, sine-modulated light beam:

$$(9) \quad g(x, t) = \alpha(1 - R)I_0 e^{-\alpha x} e^{i\omega_0 t} + G_0(x)$$

where α is the light penetration depth, R the reflection coefficient and I_0 the incident modulated photon flux. $G_0(x)$ is a homogenous generation due to biaslight and is not detected by the lock-in amplifier, so we ignore this item. The generation invokes an excess carrier density $\Delta n(x, t)$ in the p-region. Recombination in the bulk is governed by bulk lifetime τ :

$$(10) \quad r(x, t) = \frac{\Delta n(x, t)}{\tau}$$

The generated excess carriers follow the partial differential equation:

$$(11) \quad \frac{\partial}{\partial t} \Delta n(x, t) = D_n \frac{\partial^2}{\partial x^2} \Delta n(x, t) + g(x, t) - r(x, t)$$

D_n is the diffusion constant for electrons in the p region. As the carrier density $\Delta n(x, t)$ will have the same periodicity ω_0 as the generation $\Delta n(x, t)$, it can be expanded into a Fourier series

$$(12) \quad \Delta n(x, t) = \sum_{m=-\infty}^{\infty} \Delta n_m(x) \cdot e^{im\omega_0 t}$$

(12) substituted into (11) delivers an infinite, but countable set of differential equations with boundary conditions $\Delta n_m(0) = 0$ and $D_n \frac{\partial}{\partial x} \Delta n_m(W) = -S \Delta n_m(W)$

(W = cell thickness). All but one ($m=1$) of these are homogenous resulting in $\Delta n_m(x) \equiv 0$. Introducing the complex bulk lifetime $\tau^* = \frac{\tau}{1 + i\omega\tau}$, the remaining

inhomogeneous equation can be rewritten in the familiar form ($m=1$ omitted):

$$(13) \quad D_n \frac{\partial^2}{\partial x^2} \Delta n(x) = \frac{\Delta n(x)}{\tau^*} - G(x)$$

where $G(x)$ is the single Fourier coefficient of the generation.

We are more interested in the short circuit current than in the carrier concentration, which we will express in the normalised form, the internal quantum efficiency IQE:

$$(14) \quad IQE = \frac{1}{I_0(1-R)} D_n \frac{\partial}{\partial x} \Delta n(0)$$

with the solution:

$$(15) \quad IQE = \frac{L^* \cdot \left(L^* - k \frac{1}{\alpha} \right)}{L^{*2} - \frac{1}{\alpha^2}} + \frac{e^{-\alpha W} L^* \left(\left(\frac{k}{\alpha} - L^* \right) \cosh\left(\frac{W}{L^*}\right) + \left(kL^* - \frac{1}{\alpha} \right) \sinh\left(\frac{W}{L^*}\right) \right)}{L^{*2} - \frac{1}{\alpha^2}}$$

W is the solar cell thickness, α the Absorption coefficient and S the backside recombination velocity.

$$(16) \quad k = \frac{\frac{L \cdot S}{D_n} + \tanh\left(\frac{W}{L^*}\right)}{1 + \frac{L \cdot S}{D_n} \cdot \tanh\left(\frac{W}{L^*}\right)}$$

The complex diffusion length L^* is determined by

$$(17) \quad L^* = \sqrt{D_n \cdot \tau^*}$$

The phase shift φ in the lock-in measurement is introduced by the complex IQE as follows:

$$(18) \quad \tan \varphi = \frac{\text{Im}(IQE)}{\text{Re}(IQE)}$$

In our experiment, the reference frequency is around 1 kHz, and assuming $S=1000$ cm/s, the phase shift is typically around -1° , see Fig. 3. Note that the phase shift is negative, which corresponds to a retardation of the signal.

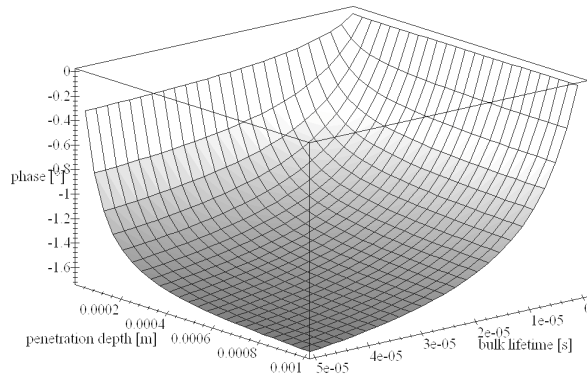


Fig. 3: LBIC phase shift introduced by carrier lifetime. Reference frequency is 1 kHz, back SRV=100 cm/s. The phase shift introduced by lifetime is negative, which corresponds to a retardation of the signal.

4.2 Phase shift introduced by capacitors and resistors

Every solar cell with space charge region incorporates a capacitance formed by the separated charges by this region. The capacitance C incorporated in a solar cell with space charge region width of 300 nm is usually around 35 nF per 1 cm². The solar cell's

capacitance does not influence DC, steady-state operation, but is very well visible in transient and AC measurements. Furthermore, non-ideal solar cells incorporate a parallel resistance R_p and a series resistance R_s . Additional series resistance may be introduced by the measurement apparatus itself.

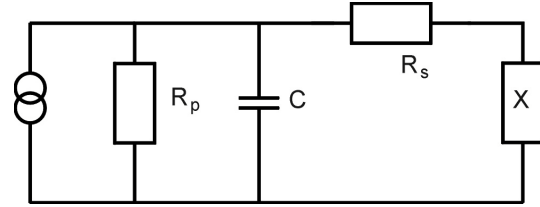


Fig. 4: simplified block diagram of a solar cell. The solar cells internal capacitor (formed by the space charge region) lies parallel to the current source and the shunt resistance. Any $X \ll \infty$ represents a load connected to the solar cell which is connected in series with the series resistance. Ideal short circuit conditions are realised by $X=0$.

The impedance Z of the diagram in Fig. 4 introduces the phase shift

$$(19) \quad \tan \varphi = \frac{\text{Im}Z}{\text{Re}Z}$$

When operating the solar cell under I_{sc} conditions and $R_s \ll R_p$, the capacitance C is connected parallel to the shunt resistor $R_s + R_M$ ($X = R_M =$ internal resistor of the measurement device), this reduces the phase to

$$(20) \quad \varphi = \arctan(\omega C(R_s + R_M))$$

In good solar cells, this is unfortunately close to zero, but the series resistance can have a strong influence when investigating bad cells.

The impedance of the diagram in Fig. 4 for V_{oc} conditions ($X = \infty$) is:

$$(21) \quad Z = R_s + \frac{1}{\frac{1}{R_p} - i\omega C}$$

When operating with a reference frequency of 1 kHz, the magnitude of the impedance $|Z_c| = \frac{1}{\omega C}$ is in the range of the parallel resistor of an industrial type solar cell ($R_p=1000-5000 \Omega\text{cm}^2$) and introduces a considerable phase shift of up to 70° . In this case, the series resistance has nearly no influence.

5 THE EXPERIMENT

As the first example, we summarise measurements of a multicrystalline industrial solar cell sized $10 \times 10 \text{ cm}^2$. The IV analysis revealed a rather high series resistance $R_s = 1.77 \Omega\text{cm}^2$ and a parallel resistance $R_p = 2022 \Omega\text{cm}^2$. Substituting the values for R_p and R_s into (21) and assuming $C = 35 \text{ nF/cm}^2$, the phase shift between V_{oc} and I_{sc}

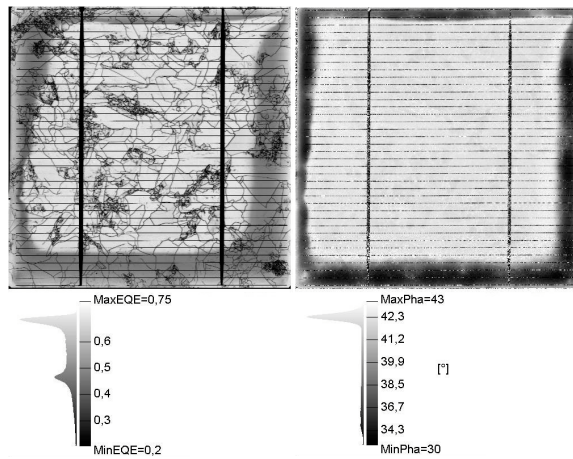


Fig. 5: EQE map (left) and phase shift map (right) of a 10*10 cm² mc solar cell operating under I_{sc} conditions. The scaling of the phase map is not linear, this improves detail recognition.

measurement should be 26° at $\omega=1.1$ kHz. We measured a phase shift of 21.3°. Both phase maps of I_{sc} and V_{oc} show a marginal phase shift of up to -4°, see Fig. 5 right. The back side of the solar cell shown in Fig. 5 is marginally covered with LPCVD silicon nitride. The sheet thickness is 70 nm maximum at the cell edges, diminishing to zero on a length of up to 2 cm. Due to backside silicon nitride coverage, no Al BSF was formed, see grey area in Fig. 5 left. Comparing the two maps, it is remarkable that the BSF uncovered region (see EQE map) and the phase shifted marginal area are not coincident. A possible explanation might be that there is a considerable contact failure in the phase shifted area, depending on rear side SiN thickness. If so, the carriers would have to spend additional time on their trip around the defect contact region, which results in a negative phase shift.

To prove this, we removed the Al contact at the upper left cell. The removal of the Al contact did not influence the EQE of the cell. As the LBIC system operates with a total optical power of 6 μ W, the generated current is only 4 μ A maximum, which is not sensitive to a prolonged current path to reach the good contact area. The phase map of the removed Al contact shows an additional phase shift of -2° in the areas with no BSF, whereas the BSF covered areas remain unchanged. As a result, the phase map can at least detect a contact failure in the non-BSF covered region, which is not visible in the EQE map.

The second example is a 5*5 cm² solar cell with backside Al grid and screen printed emitter. For details of the production of this solar cell see [10]. The diffusion behaviour of the phosphorus paste leads to a backside collecting emitter in some regions of the solar cell. In the EQE map, this regions are hardly visible, whereas in the phase map they're clearly visible as a phase shift (dark grey regions in Fig. 6 right). The phase shift comes from the fact that the backside collecting emitter is connected to the frontside emitter only across the solar cell's edges. The prolonged travelling path in the emitter invokes the phase shift.

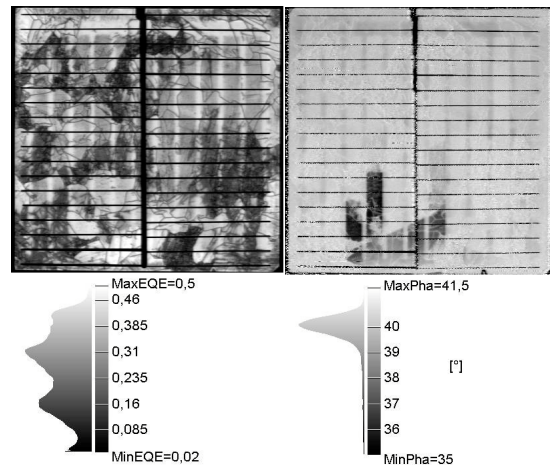


Fig. 6 : EQE map (left) and phase map (right) of a 5*5 cm² solar cell with backside Al grid and screen printed emitter.

6 CONCLUSION

Every LBIC system using lock-in amplifiers can detect the phase shift of the signal. By recording the phase shift of both V_{oc} and I_{sc} measurements one can get additional information about local impedances, hints on abnormal contact properties and the carrier collecting velocity. In the experiments, the analysis of the phase shift revealed additional information which was not clearly visible in the phase-independent EQE maps.

ACKNOWLEDGEMENTS

We would like to thank B. Fischer and K. Faika for the fruitful discussions on the topic. This work was supported by the E.C. within the Fast-IQ project under contract No. ERK6-CT1999_00002.

REFERENCES

- [1] F. Sanii et al., Proc. 20th IEEE Photov. Spec. Conf. 1988, p. 575-580
- [2] T. Pernau et al., Proceedings of the 17th EPSEC, München 2001, VD 1.4 (to be published)
- [3] M. Acciarri et al., Mater. Sci. Eng., B42 (1996) 208.
- [4] G. Agostinelli et al., Proceedings of the 2nd WCPEC, Vienna, Austria, 1998, p. 184.
- [5] G. Agostinelli et al., 'Large Area Fast LBIC as a Tool for Inline PV Modula and String Characterisation', 17th EPSEC, München 2001, OA 1.2 (to be published)
- [6] M. Stemmer, Appl. Surf Sci. **63** (1993), 213-217
- [7] J. Carstensen et al., Proc.16th EPSEC, Vol. II, p. 1627-1630
- [8] J. Bajaj et al., J. Vc. Sci. Technol. A 5(5), Sept/Oct 1987, 3186-3189
- [9] W. Warta et al., Proc. 2nd WCEPSEC, Wien, 1650 (1998)
- [10] K. Faika et al., 'Formation of a Rectifying p+ n+ Junction Using P-Paste During Al/P-Codiffusion' V2.5, this conference
- [11] www.lockin.de